REGULAR ARTICLE

blood advances

Fibrin protofibril packing and clot stability are enhanced by extended knob-hole interactions and catch-slip bonds

Nathan L. Asquith,[1,2] Cédric Duval,[1] Artem Zhmurov,[3-5] Stephen R. Baker,[1] Helen R. McPherson,[1] Marco M. Domingues,[1,6] Simon D. A. Connell,[7] Valeri Barsegov,[8] and Robert A. S. Ariëns[1]

[1]Discovery and Translational Science Department, Leeds Institute of Cardiovascular and Metabolic Medicine, School of Medicine, University of Leeds, Leeds, United Kingdom; [2]Vascular Biology Program, Karp Research Laboratories, Boston Children's Hospital, Harvard Medical School, Boston, MA; [3]The EuroCC National Competence Center Sweden, Stockholm, Sweden; [4]PDC Center for High Performance Computing, KTH Royal Institute of Technology, Stockholm, Sweden; [5]Science for Life Laboratory, Solna, Sweden; [6]Institute of Molecular Medicine, Faculty of Medicine, University of Lisbon, Lisbon, Portugal; [7]Molecular and Nanoscale Physics Group, School of Physics and Astronomy, University of Leeds, Leeds, United Kingdom; and [8]Department of Chemistry, University of Massachusetts, Lowell, MA

Key Points

- Mutations of residues responsible for extended knob-hole interactions in fibrin result in altered clot formation, structure, and mechanics.
- Molecular dynamic simulations show that only slip bonds occur in mutant systems, whereas catch-slip bonds are present in wild-type fibrin.

Fibrin polymerization involves thrombin-mediated exposure of knobs on one monomer that bind to holes available on another, leading to the formation of fibers. In silico evidence has suggested that the classical A:a knob-hole interaction is enhanced by surrounding residues not directly involved in the binding pocket of hole a, via noncovalent interactions with knob A. We assessed the importance of extended knob-hole interactions by performing biochemical, biophysical, and in silico modeling studies on recombinant human fibrinogen variants with mutations at residues responsible for the extended interactions. Three single fibrinogen variants, γD297N, γE323Q, and γK356Q, and a triple variant γDEK (γD297N/γE323Q/γK356Q) were produced in a CHO (Chinese Hamster Ovary) cell expression system. Longitudinal protofibril growth probed by atomic force microscopy was disrupted for γD297N and enhanced for the γK356Q mutation. Initial polymerization rates were reduced for all variants in turbidimetric studies. Laser scanning confocal microscopy showed that γDEK and γE323Q produced denser clots, whereas γD297N and γK356Q were similar to wild type. Scanning electron microscopy and light scattering studies showed that fiber thickness and protofibril packing of the fibers were reduced for all variants. Clot viscoelastic analysis showed that only γDEK was more readily deformable. In silico modeling suggested that most variants displayed only slip-bond dissociation kinetics compared with biphasic catch-slip kinetics characteristics of wild type. These data provide new evidence for the role of extended interactions in supporting the classical knob-hole bonds involving catch-slip behavior in fibrin formation, clot structure, and clot mechanics.

Introduction

Fibrin polymerization is a key process in hemostasis that provides a protein scaffold for the blood clot to stem bleeding. Fibrin(ogen) also plays a role in atherothrombosis,[1] venous thromboembolism,[2] angiogenesis,[3] and infection control.[4,5] Fibrinogen is comprised of 3 pairs of polypeptides ($A\alpha_2B\beta_2\gamma_2$), linked by disulphide bonds forming a trinodular elongated protein.[6,7] The N termini of all chains begin in the central E-region and extend outward in a coiled coil to two distal D-regions. The Bβ- and γ-chains terminate in

Submitted 4 January 2022; accepted 3 May 2022; prepublished online on *Blood Advances* First Edition 13 May 2022; final version published online 8 July 2022. DOI 10.1182/bloodadvances.2022006977.

Requests for data sharing may be submitted to Robert Ariëns (r.a.s.ariens@leeds.ac.uk).

The full-text version of this article contains a data supplement.

the D-region, whereas the longer flexible Aα-chain folds backward along the coiled coil toward the E-region.[8]

The conversion of fibrinogen to fibrin is facilitated by thrombin, which cleaves 2 fibrinopeptides, A (FpA) and B (FpB), from the N termini of the Aα- and Bβ-chains, respectively.[9] The removal of FpA and FpB exposes knobs A and B on one fibrin monomer that spontaneously bind to permanently exposed holes a (in the γ-chain) and b (Bβ-chain) on another monomer, respectively,[10-12] forming half-staggered fibrin oligomers.[13] Polymerization continues, forming larger species of oligomers termed protofibrils. On reaching a length of ~0.5 μm, protofibrils aggregate laterally to form fibers.[14] The current view of fibrin polymerization dynamics is that A:a knob-hole interactions drive longitudinal growth, which results in formation of oligomers and protofibrils, whereas the B:b knob-hole and α-chain connector interactions are responsible for lateral aggregation.[15-24]

Evidence suggests that A:a interactions involve additional residues beyond the traditional binding pocket (hole a). The synthetic knob A peptide GPRP (Gly-Pro-Arg-Pro), used to recapitulate knob A, weakly binds with hole a in cross-linked double-D fragment (K_d of 25 μM),[12] whereas larger fibrin fragments bind ~5 times more tightly with fibrinogen (K_d of 5.8 μM).[25] This provides evidence that additional residues beyond the classical A:a interaction sites contribute to knob-hole coupling. Recent all-atom molecular dynamic (MD) simulation studies provide further evidence that extended interactions occur near the A:a interface,[26] indicating that A:a interactions are enhanced by electrostatic interactions between γGlu323/βLys58, γLys356/βAsp61, and γAsp297/βHis67. Furthermore, a recent study combining single-molecule forced dissociation by atomic force microscopy (AFM) with MD simulation-based molecular modeling revealed biphasic catch-slip kinetics of A:a knob-hole bond rupture.[27] Dynamic pulling force-induced remodeling of the A:a association interface provided a molecular mechanism underlying such dual-catch-slip response to external mechanical factors.

This body of evidence from experimental and computational modeling studies indicate the existence of additional contacts between residues outside the immediate A:a interface, which might also become activated mechanically. However, no studies have hitherto explored the effects of mitigation of catch-slip-type dynamics in knob-hole interactions on the kinetics of fibrin polymerization and resulting clot structure. To better understand the role of these additional interactions, we produced 4 recombinant human fibrinogens with mutations in the extended interaction sites, γD297N, γE323Q, and γK356Q, and a γDEK variant combining all 3 mutations. We investigated fibrin polymerization and clot structure in conjunction with MD simulations of atomic structural models of the A:a knob-hole complexes. Our studies reveal that γD297 and γE323 are important elements in the transition of the A:a knob-hole interactions from catch to slip bonds, whereas γK356 is primarily involved in the lateral packing interactions at the protofibril level. All variants altered fiber packing and structure, whereas the γDEK variant also altered clot density and mechanics. These data demonstrate a key role for extended knob-hole interactions and catch-slip bonds in fibrin formation, clot structure, and clot mechanical properties. It is understood that fibrin biomechanics are important for clot stability in thrombosis,[28,29] therefore, these findings have important implications for thromboembolic diseases.

Methods

Recombinant fibrinogen expression

To disrupt electrostatic interactions because of multiple binary contacts between residues preceding knob A and residues in the γ-nodule outside the binding pocket,[26] we selected amino-acid substitutions neutralizing side-chain charge: negatively charged Asp to neutral Asn (γD297N); negatively charged Glu to neutral Gln (γE323Q); and positively charged Lys to neutral Glu (γK356Q). The expression and purification of recombinant human fibrinogen has been described previously.[4,30] Single-point mutations γD297N, γE323Q, and γK356Q, and triple-point mutation γD297N/γE323Q/γK356Q (γDEK) were created by site-directed mutagenesis of the pMLP (major late promoter) expression vector containing the fibrinogen γ-chain sequence[30] (see supplemental Table 1). Recombinant wild-type (WT) protein was also produced. All constructs were confirmed by sequencing and cotransfected with selection plasmid pMSV-His into CHO (Chinese Hamster Ovary) cells already overexpressing fibrinogen Aα and Bβ chains. Clone selection, expression, and purification were performed as described in the supplemental Methods.

Turbidity

Polymerization of fibrin variants (0.5 mg/mL fibrinogen, 5 mM $CaCl_2$, and 0.1 U/mL thrombin [TBS]) (Tris-buffered saline) was analyzed in 384-well plates (Greiner, Stonehouse, UK) using a Powerwave microtiter-plate reader (Bio-Tek, Swindon, UK) as previously described.[31] Optical density was measured ($\lambda = 340$ nm) every 12 seconds for 2 hours at 37°C. Three outputs were analyzed from the turbidity profiles: lag phase, maximum optical density (MaxOD), and maximum polymerization rate. Additional turbidity measurements were performed using 0.5 BU/mL reptilase (final concentration) to cleave fibrinopeptide A only.

AFM

AFM was used to study early protofibril formation as previously described[17,32] (see supplemental Methods). The polymerization components of the reaction were reduced to focus on the early stages of polymerization.

Confocal and electron microscopy

Fibrin clot structure was analyzed by laser scanning confocal microscopy and scanning electron microscopy (SEM) as described[4,30] (see supplemental Methods). Fibrinolysis was studied by confocal microscopy (see supplemental Methods). Polymerization conditions for SEM are chosen as they allow for polymerization of clots that are strong enough to withstand mechanical forces applied to them during the EM sample preparation process.

Protofibril packing

Fibrin clots (0.5 mg/mL fibrinogen, 5 mM $CaCl_2$, and 0.1 U/mL thrombin; TBS) were formed in a polystyrene cuvette (Eppendorf, Stevenage, UK) and immediately sealed with parafilm to prevent dehydration. The clots were formed overnight at room temperature. After clot formation, the clots were scanned between $500 < \lambda < 800$ nm in a Λ35 UV-Vis spectrophotometer (Perkin-Elmer, Cambridge, UK). The average fiber diameter, number of protofibrils, and protofibril distribution within a fiber were determined from the wavelength dependent turbidity of fibrin clots as described.[32-34]

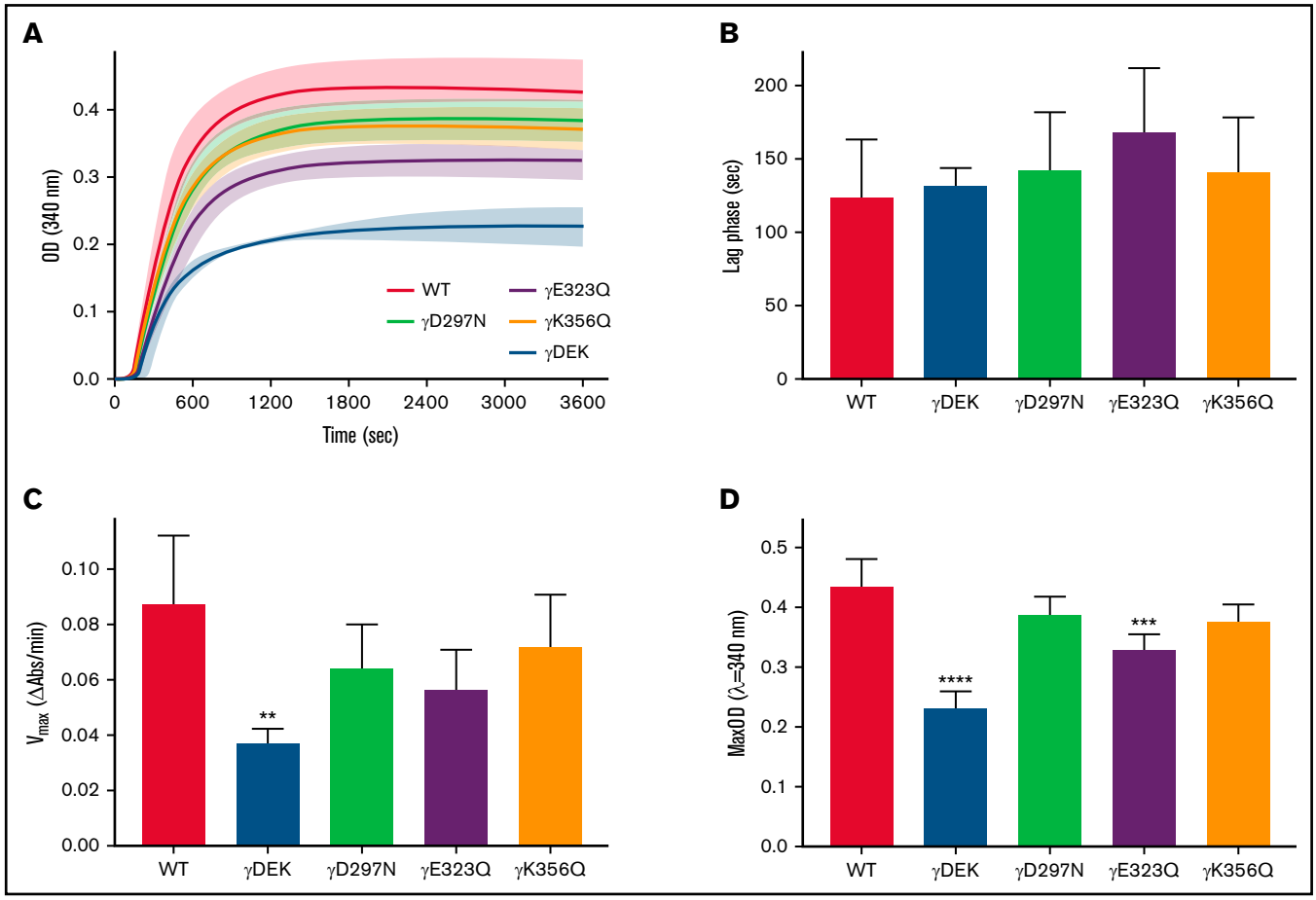

Figure 1. Recombinant fibrinogen variants γDEK, γD297N, γE323Q, and γK356Q corresponding to extended knob-hole interactions affect fibrin polymerization. (A) Polymerization curves, (B) lag phase duration, (C) polymerization rate V_{max}, and (D) maximum optical density, MaxOD for all variants and WT fibrinogens. Mean ± standard deviation (SD), N = 3 (γDEK), N = 4 (single variants). $^{**}P < .01$; $^{***}P < .001$, $^{****}P < .0001$ compared with WT.

Micro-rheology of fibrin clots

An in-house micro-rheology device (magnetic tweezers) was used to assess the viscoelastic properties of WT and variant clots as previously described[32,35] (see supplemental Methods).

Atomic structural models

Atomic structures of the WT fragment D with hole a (residues γCys139-Val411) and hole a with single-point mutations (γD297N, γE323Q, γK356Q, and γDEK) co-complexed with knob A (residues αGly17-Cys36) were extracted from the structural models of fibrin oligomers.[6,36] Atomic models with single point mutations were reconstructed in silico by replacing the corresponding amino-acids, that is, γAsp297toAsn (γD297N), γGlu323toGln (γE323Q), and γLys356toGln (γK356Q). The triple mutant γDEK was reconstructed by introducing all three mutations described above. The obtained models of WT and variant A:a knob-hole complexes were energy minimized, using the steepest descent algorithm, and equilibrated at 25°C with the harmonic constraints imposed on the backbone atoms.

Dynamic force experiments in silico

Due to large system size (entire A:a knob-hole bond complex) and long timescale involved (microseconds), we used GPU-accelerated[37,38] all-atom MD simulations in implicit water with the solvent accessible surface area (SASA) model of implicit solvation in conjunction with CHARMM19 force field.[39] For each model system (γD297N, γE323Q, γK356Q, and γDEK), five independent runs (each of ∼1-μs duration) of stirred MD simulations were performed. To mimic the experimental AFM measurements, in these simulations, we used the following force protocol: (1) pulling force was applied in the direction perpendicular to the A:a association interface to rupture the A:a bond; (2) the C_α-atom of γLys159 in the γ-nodule (hole a) was constrained; and (3) the C_α-atom of αCys36 (knob A) was tagged through the harmonic spring with stiffness $k = 100$ pN/nm (virtual cantilever). We used the low-friction limit with damping coefficient of 2.0 ps^{-1}. This does not alter the thermodynamics of noncovalent interactions and allows for more efficient sampling of the conformational space. Profiling the average bond lifetime of noncovalent bonds in the constant-force pulling simulations (force-clamp assays) is computationally expensive, and therefore we used the dynamic force-ramp. To mimic the dynamic force-ramp conditions used in single-molecule experiments on protein-protein complexes and to probe the tension-dependent strength of the A:a knob-hole bond, the applied pulling force $f = r_f t$ was ramped up with the pulling speed of $v_t = 10^4$ μm/s. This corresponds to a force-loading rate of $r_f = kv_t = 10^{-3}$ N/s.

Results

Recombinant fibrinogens

Sodium dodecyl sulfate-polyacrylamide gel electrophoresis of WT and mutant fibrinogens is shown in supplemental Figure 1. The gel demonstrates bands representative of fibrinogen Aα-, Bβ-, and γA-chains at their expected molecular weights. No additional bands were observed, indicating that the samples were homogeneous and did not contain degradation products.

Extended knob-hole variants increase polymerization rate

There were differences in the polymerization profiles between variant and WT fibrinogens (Figure 1A). Lag phase was similar for all variants compared with WT (Figure 1B). However, maximum polymerization rate V_{max} was reduced for all variants compared with WT and significantly so for γDEK (−57%, $P < .01$; Figure 1C). All variants showed reduced maximum OD compared with WT, which was significant for γDEK (−47%, $P < .0001$) and γE323Q (−25%, $P < .001$; Figure 1D). Protofibril growth across the variants was determined using AFM (supplemental Figure 2). The average protofibril length for γD297N (−20%, $P < .05$) and γK356Q (+15%, $P < .05$) was significantly different from the WT 10 minutes after fibrin polymerization was initiated (Table 1). A similar turbidity profile was observed for WT and recombinant variants when using reptilase for FpA cleavage only (supplemental Figure 3), indicating that observed effects are because of changes in knob-hole binding rather than thrombin affinity.

Clot structure is influenced by extended knob-hole variants

Next, we analyzed clot density under hydrated conditions using laser scanning confocal microscopy. Clots obtained from γDEK fibrinogen (Figure 2) were significantly denser than those from WT (+39%, $P < .001$; Figure 2). Visual inspection of the density by scanning electron microscopy of fibrin clot networks at ×20 000 magnification (Figure 3A-E) also displayed a similar trend. All variants resulted in formation of clots with more densely packed fibers characterized by reduced apparent fiber diameter (Figure 3F). No significant differences were observed for fibrinolysis for any of the fibrin clots (supplemental Figure 4).

Protofibril packing is increased by extended knob-hole variants

Interestingly, light scattering analysis of fibrin fiber packing demonstrated that extended knob-hole variants led to no apparent change in fiber diameter under fully hydrated conditions, compared with WT (Figure 4A). However, a reduction in average number of protofibrils per fibrin fiber was observed for the recombinant variants (Figure 4B) and was associated with increased distance between individual protofibrils within individual fibers (Figure 4C).

Table 1. Average protofibril lengths

	10 min	20 min
WT	190 ± 71 nm	250 ± 147 nm
γDEK	163 ± 54 nm	221 ± 128 nm
γD297N	152 ± 73 nm*	291 ± 191 nm
γE323Q	184 ± 82 nm	256 ± 163 nm
γK356Q	218 ± 110 nm*	286 ± 134 nm

Results are presented as mean ± standard deviation. Greater than 20 protofibrils were measured per condition over 3 independent experiments.
*$P < .05$ vs WT at the same time point.

Extended knob-hole variants support clot mechanics

The viscoelastic properties of fibrin clots were analyzed using magnetic tweezers. The loss tangent (Tan[δ] = G″/G′) was calculated at different frequencies to determine the deformation of clots. Three frequencies (0.1, 1, and 10 Hz; Figure 5A-C) were chosen based on deformation events that occur in fibrin networks.[32] Tan[δ] at low frequencies represents deformation that occur at the whole clot level, whereas the intermediate-to-high frequency ranges represent deformation at the fibrin fiber level. At 0.1 Hz (Figure 5A), tan[δ] was significantly increased for γDEK (+131%, $P < .001$) compared with WT, showing that these clots were more readily deformable.

Structural insights from atomic models of fibrin oligomers

Single-point mutations γD297N, γE323Q, and γK356Q are located at the previously identified important binding regions inside and around the binding pocket (hole a), namely in the movable flap (γD297N), loop I (γE323Q), and interior region (γK356Q) (Figure 6). We analyzed the atomic structures of fibrin oligomers and protofibrils reported previously[6,36] to estimate the propensities of these residues to form intra- vs inter-protofibril contacts. We found the following: (1) position γ297 in the movable flap is buried in the protofibril, and therefore this residue can mediate formation of the intra-protofibril contacts (promoting the longitudinal growth) but not inter-protofibril contacts; (2) position γ323 in loop I is somewhat exposed to solvent, and hence, this residue can potentially form intra-protofibril contacts and inter-protofibril contacts (promoting lateral packing); and (3) position γK356Q is in the solvent accessible area but far from knob A, and therefore this residue can participate in formation of inter-protofibril contacts.

Extended interactions strengthen knob-hole bonds

Next, we carried out MD simulations, in which pulling force was applied to knob A to dissociate the A:a bond (Figure 6). The profiles of unbinding force, binding affinity Q, and peak rupture force f were used to investigate the dynamics of bond rupture. The unbinding force quantitates instantaneous mechanical tension in the noncovalent A:a bond. The binding affinity Q reflects the strength of the noncovalent A:a bond. The peak rupture force f corresponds to the tension threshold at which the A:a bond dissociates. The profiles of Q vs f in supplemental Figure 5 show 2 different scenarios: (1) Q first increases and then decreases with force f (catch-slip bond character), and (2) Q decreases monotonically with f (slip bond character). Both catch-slip and slip scenarios were observed for WT and mutants γK356Q, and only slip scenario was observed for mutants γD297N, γE323Q, and γDEK (Figure 7). Therefore, in agreement with insights from the atomic structural models, MD simulations showed the following: (1) the A:a bond weakens and hence dissociates at lower f = 60- to 90-pN rupture force for fibrinogen variants γD297N, γE323Q, and γDEK (in all 5 simulation runs) compared with higher 90- to 120-pN rupture force for WT (from 5

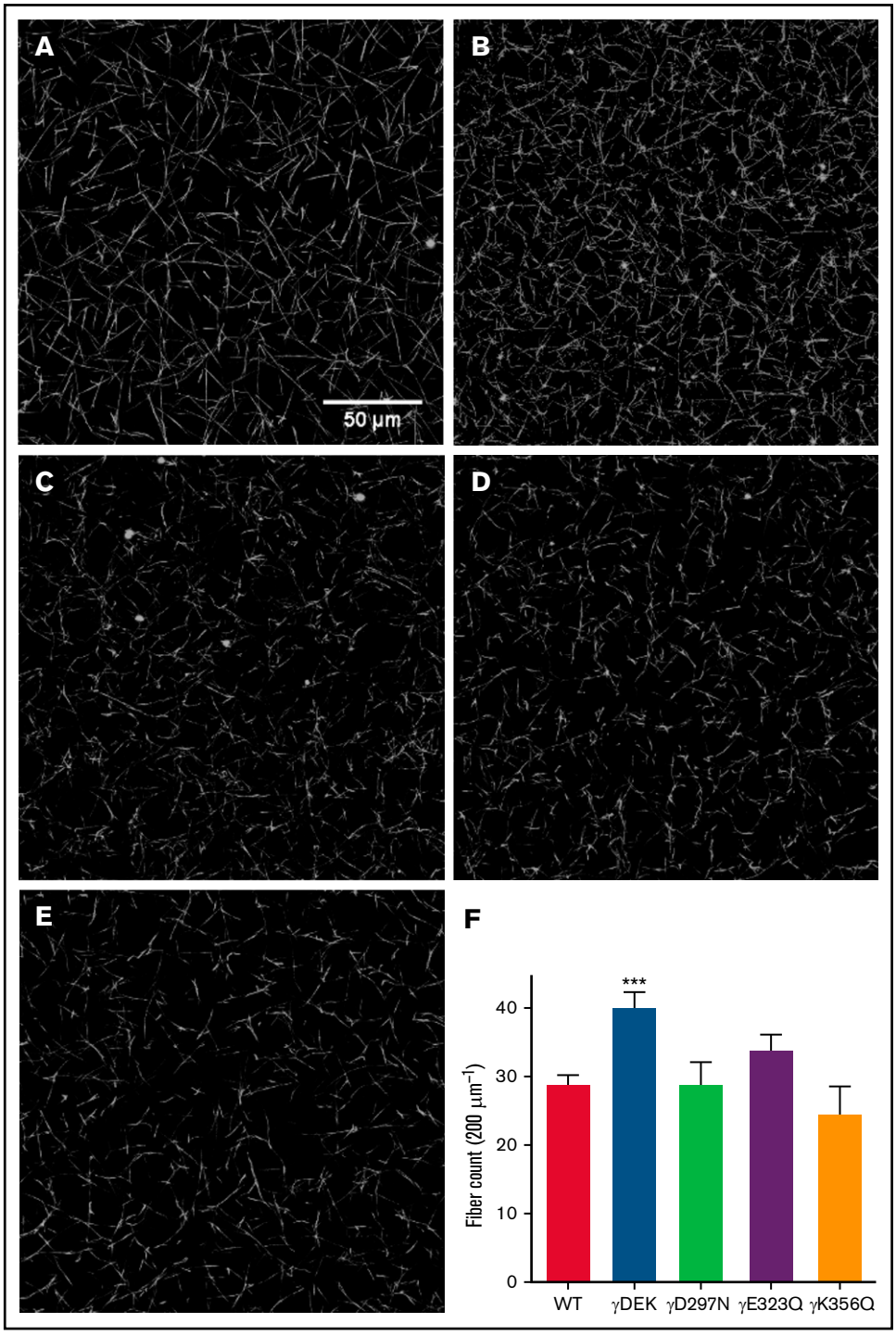

Figure 2. Density differences of WT and fibrinogen variant fibrin clots involved in extended knob-hole interactions. Fibrin clots were allowed to form for 1 hour and imaged using laser scanning confocal microscopy (A: WT, B: γDEK, C: γD297N, D: γE323Q, E: γK356Q). Fiber count per 200 µm was quantified (F). Variant γDEK (B, F) was denser than WT (A, F). Mean ± SD, N = 4 (WT), N = 3 (all variants). ***$P < .001$ for variants compared with WT.

control runs); and (2) the A:a bond weakens (60- to 90-pN rupture force) in 1 of 5 runs and does not change in 4 of 5 runs for fibrinogen γK356Q (supplemental Figure 5). In γD297N, γE323Q, and γDEK, the movable flap did not translocate toward knob A (Figure 7) and therefore did not facilitate additional stabilization to the A:a bond (low-affinity bound state, slip bond character). Hence, mutations in the movable flap (γD297N) and loop I (γE323Q) weaken the A:a bond by about 30 pN. This also explains similar results for triple mutant γDEK (reduced f = 60- to 90-pN rupture force). Mutation γK356Q had less-pronounced effects on the

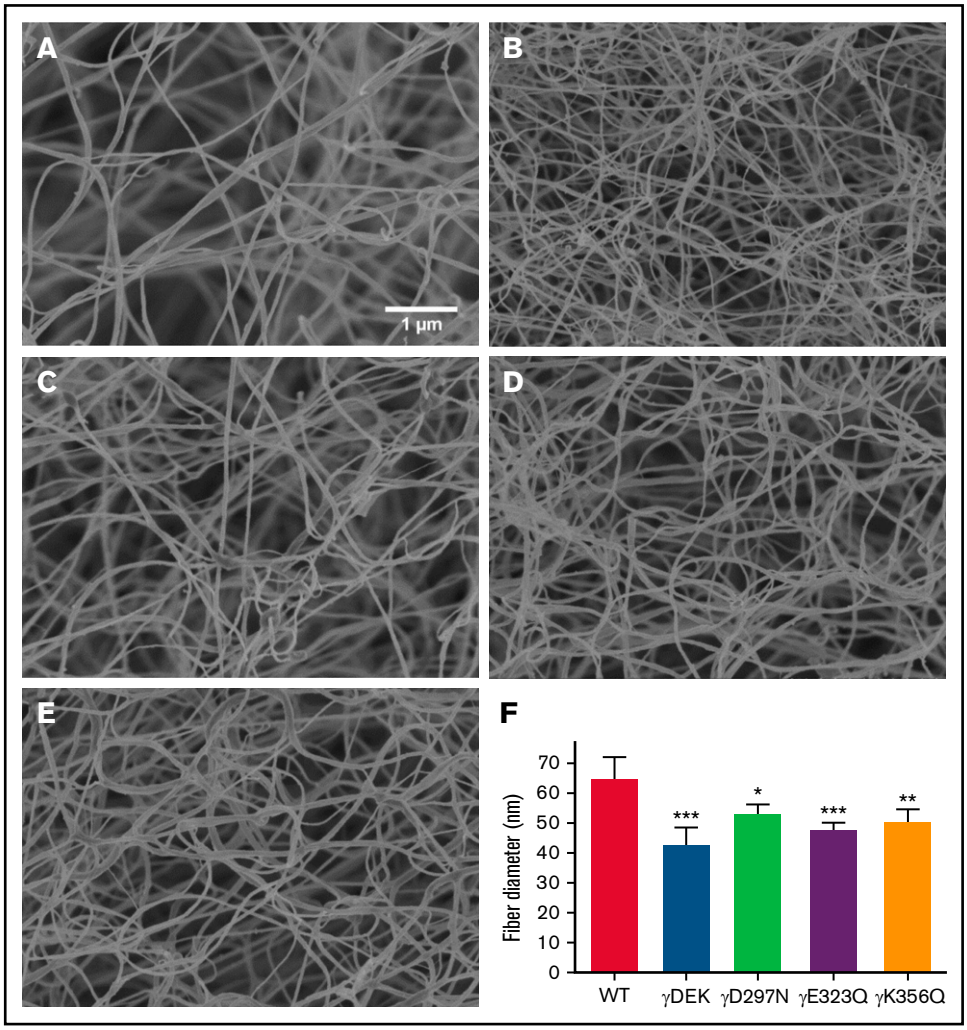

Figure 3. Recombinant fibrinogen variants γDEK, γD297N, γE323Q, and γK356Q affect fiber thickness. Micrographs were taken at ×20 000 magnification using a Hitachi SU8230 scanning electron microscope (A-E). Compared with WT (A), fibrin fibers of γDEK (B, F), γD297N (C, F), γE323Q (D, F), and γK356Q fibers (E, F) were thinner. Mean ± SD, N = 3 (WT, γDEK, γD297N), N = 4 (γK356Q), N = 5 (γE323Q). *$P < .05$; **$P < .01$; ***$P < .001$ compared with WT.

strength of A:a knob-hole bonds, in agreement with structural insights from the atomic models of fibrin oligomers and protofibrils.[6,36] The profiles for the average rupture force (Figure 6) summarizes these results, namely the weakening of A:a knob-hole bonds for γD297N, γE323Q, and γDEK variants but near-normal bond for γK356Q.

Extended knob-hole interactions enhance formation of catch bonds

A recent study has shown unique and characteristic catch-slip bond behavior for A:a knob-hole interaction.[27] Interactions between residues in knob A and residues mainly in the movable flap and, to some extent, in loop I were shown to define dynamic transition from catch to slip bond. In our simulations, the tension-induced strengthening can be detected by analyzing, for example, the pulling force-dependent profiles of the total number of knob-hole residue-residue contacts, which we refer to as binding affinity *Q*. By multiplying *Q* by the average contact energy, we obtain the binding energy of the A:a knob-hole interaction.

The force-dependent profiles of *Q* showed initial increase in *Q* (high-affinity catch-bond character) in 3 of 5 runs for WT fibrinogen and 1 of 5 runs for mutation γK356Q (supplemental Figure 5). Here, the movable flap extended toward knob A, thus forming additional knob-hole binding contacts between residues γ297-γ304 in the movable flap and residues α17-α22 in knob A (Figure 7). This provides structural support for tension-dependent A:a knob-hole bond stabilization, which results in hole a closure and formation of high-affinity bound state (catch bond). However, for γD297N, γE323Q, and γDEK, *Q* progressively decreased with force to 0, which corresponds to complete knob-hole bond dissociation, showing the absence of catch-bond formation. Here, negatively charged residues Asp γ291, γ294, γ297, and γ301 in the movable flap (γ291, γ294, and γ301 for γD297N) form strong electrostatic contacts with the positively charged residues Arg γ256 and γ275 in the γ-nodule (supplemental Figure 7). Hence, there is no tension-induced bond stabilization, and only a low-affinity bound state is formed for γD297N, γE323Q, and γDEK (slip bond character).

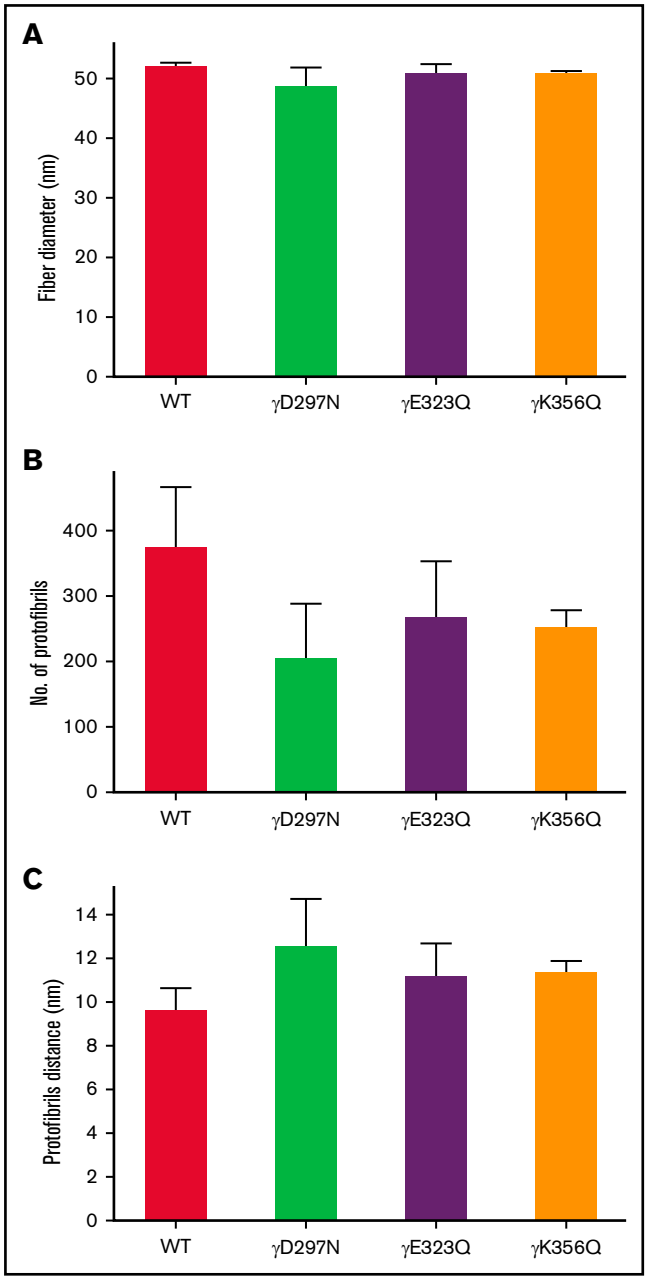

Figure 4. Protofibril packing dynamics of WT and extended knob-hole variant fibrin fibers. The UV-Vis spectrum (500 nm $< \lambda <$ 780 nm) of fibrin clots was scanned for WT and all variants. The wavelength dependent turbidity of the fibrin clots was used to determine fiber diameter and quantitate intrafibrillar protofibril packing arrangements. The fiber diameter (A) corresponding to all 4 variants were similar to WT, and the number of protofibrils per fiber (B) was reduced for all variants, resulting in an increase in the distance between protofibrils (C). Mean ± SD, N = 3.

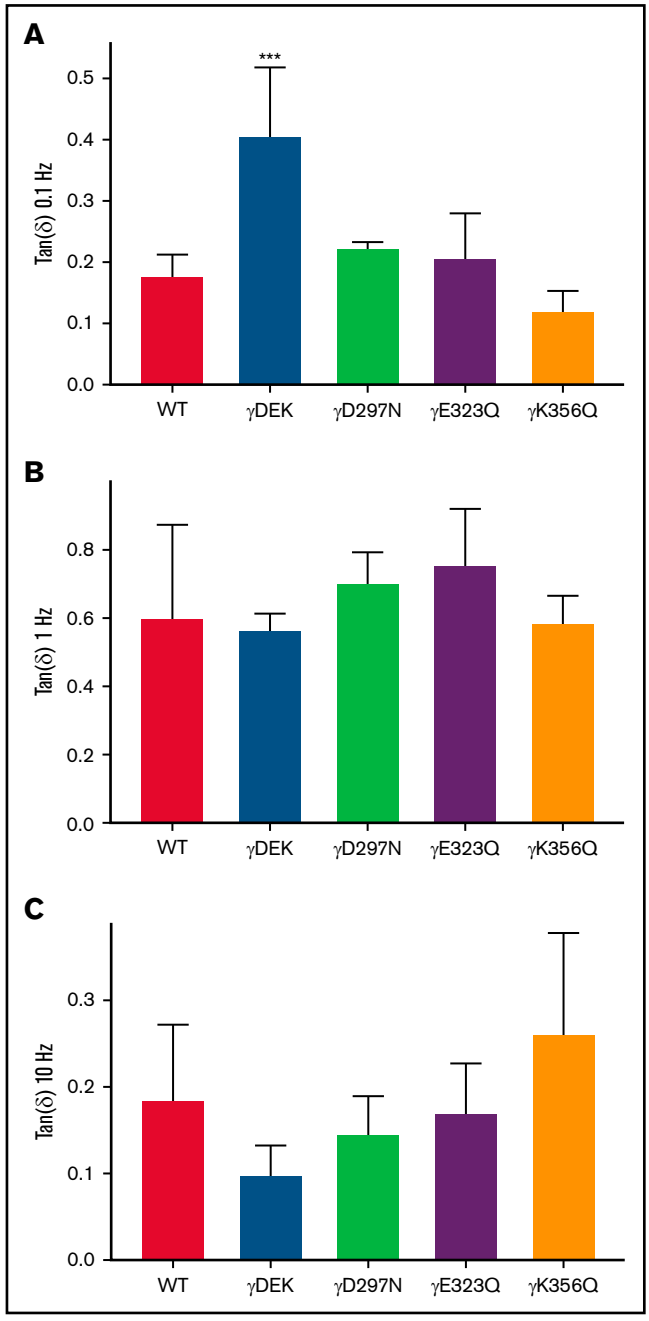

Figure 5. Extended knob-hole interactions affect overall visco-elastic properties of the clot (tanδ). Micro-rheology experiments were conducted by forming a fibrin clot in a capillary tube. Tan[δ] at 0.1 Hz (A) was significantly increased for γDEK, whereas the single variants were similar to WT. At 1 Hz (B) and 10 Hz (C), [tanδ] was similar to WT for all variants. Mean ± SD, N = 3. ***$P < .001$ compared with WT.

Discussion

The all-atom MD simulations carried out in this study provide evidence for possible location of extended knob-hole interactions,[26] previously postulated by others.[40] To test these proposed interaction sites, we produced 4 fibrinogens with mutations in each or all 3 ion-pairing residues that underpin the proposed extended binding. Our study shows that the catch-slip bond behavior of knob A with hole a can be disrupted by variants γD297N, γE323Q, and γDEK that flank the binding pocket. The change in the strength of A:a knob-hole bond and hence the kinetic of binding of knob A to hole a result in reduced fiber growth and decreased protofibril packing, leading to denser clots with reduced fiber mass-length ratio. Changes to residue γK356 involved in lateral inter-protofibril

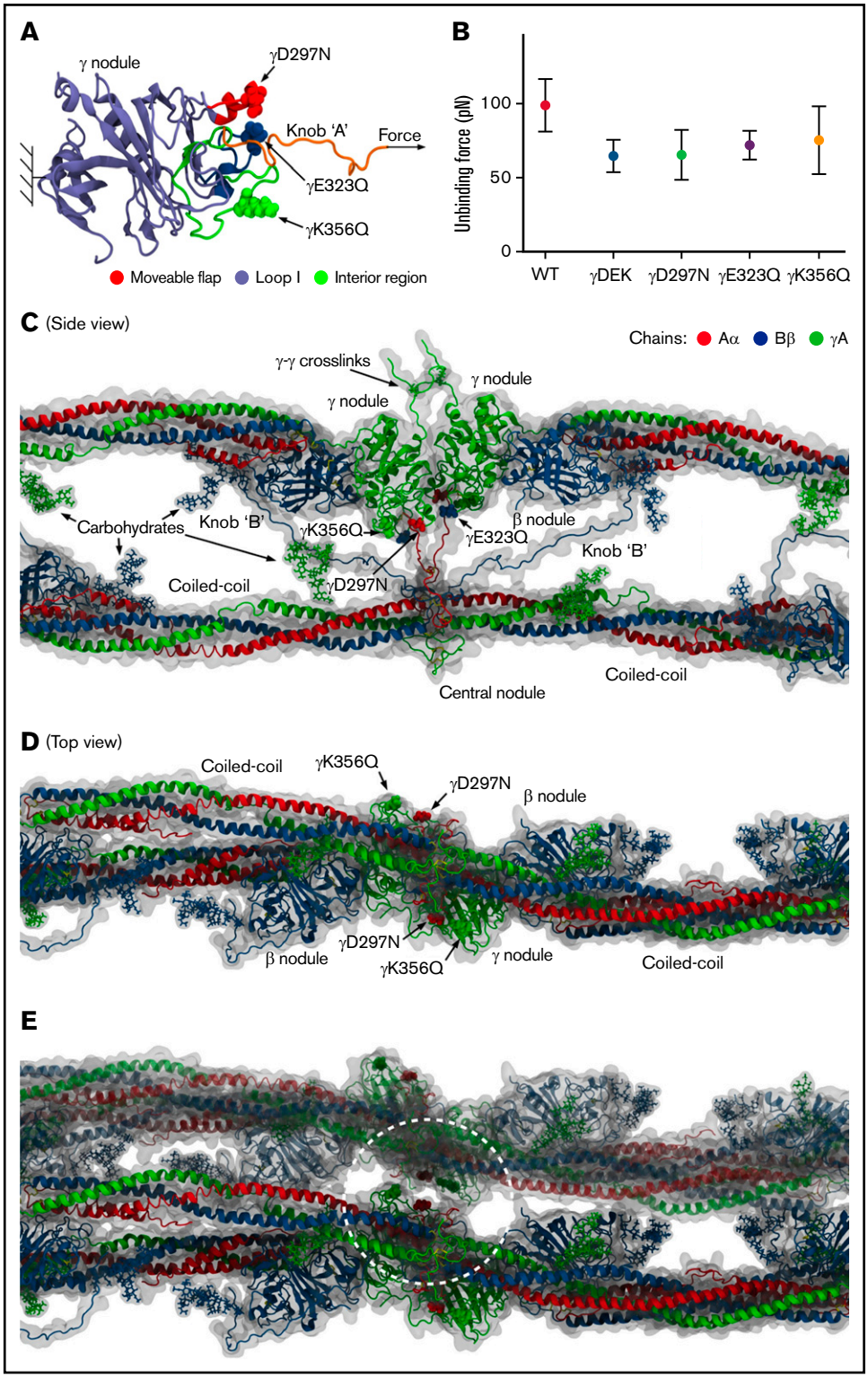

Figure 6. Computational molecular modeling. (A) Complete atomic structure of the A:a knob-hole complex (in ribbon representation), extracted from the structures of fibrin oligomers[6,36] at pH 7.0 and 25°C, showing hole a with the following binding determinants: the interior region (residues γTrp335-Asn365; shown in green), loop I (γTrp315-Trp330; in blue), and movable flap (γPhe295-Thr305; in red) in the γ-nodule, and knob A (residues αGly17-Cys36; shown in orange). Also shown are the setup for the dynamic force experiments in silico, for example, the constrained residue γLys159 in the γ-nodule in hole a and tagged residue αCys36 in knob A, and the direction of pulling force (indicated by the arrow), and single-point mutations corresponding to variants γD297N, γE323Q, and γK356Q (small arrows). (B) The average bond-rupture forces and SDs (mean ± SD, N = 5 simulation runs) for WT and variants γD297N. γE323Q, γK356Q, and γDEK extracted from the simulations. (C-D) The side view

interactions also caused delayed protofibril formation, decreased protofibril packing, and reduced mass-length ratio. The changes from catch-slip to slip character for the A:a bond and disruption of packing interactions in γDEK caused an increase in overall clot deformability, despite a denser clot network. These data show that extended knob-hole interactions are essential for the formation of catch-slip type A:a bonds and for the assembly of fibrin clots resistant to plastic deformation.

Turbidity analysis showed a decrease in maximum OD for all variants, which is reflective of denser clot networks comprised of fibers with reduced mass-length ratio.[14,33,41,42] These changes in clot structure were confirmed by confocal microscopy (clot density) and SEM (fiber diameter). Typically, fibrin clots that are highly branched, with high fiber counts and small pores are considered prothrombotic[43] and are associated with high thrombin[44] and high fibrinogen concentrations.[45] These observations suggest that the reduction in average protofibril number packed per fiber for the variants used in this study enables the presence of free protofibrils that are able to readily form additional fibrin fibers and a denser clot network.

The calculation of fibrin radii using light scattering[33,34] does not require sample preparation, compared with SEM which requires fixation and dehydration of samples.[32] Our results show that the abolition of extended A:a knob-hole interactions resulted in reduced protofibril packing. Analysis of fibers by turbidimetry showed diameters that were ∼3 times larger than those measured by SEM. Dehydration during SEM sample preparation may impact the final micrographs, as fibers are comprised of ∼20% protein and ∼80% water.[46] Because of this high-water content, fibrin fibers behave like a hydrogel.[47] For densely packed fibers, less contraction occurs during dehydration, but for less densely packed fibers, this contraction may be larger, leading to thinner fibrin fibers.[32] Therefore, abolition of extended knob-hole interactions in the variants lead to reduced protofibril packing and fibers with reduced mass-length ration in SEM and light scattering experiments.

Longitudinal protofibril growth analyzed by AFM was reduced for γD297N and increased for γK356Q after 10 minutes of clotting. The initial delay in protofibril growth for γD297N may result from the absence of A:a catch bonds, which would reduce the stability of forming oligomers and would impact lateral protofibril aggregation. The resulting clots would therefore be structurally different from WT clots. In contrast, γK356Q displayed longer protofibrils after 10 minutes. It was previously suggested that residue γK356 is in a region functionally important for lateral γ-nodule packing interactions.[19] Disturbance in lateral packing may allow for the formation of longer rather than thicker protofibrils for γK356Q. It is possible that the protofibril length for polymerizing γDEK fibrin was not different because the enhancement of protofibril length from γK356Q counteracted the reduction in length induced by γD297N.

The fibrin network provides mechanical strength to withstand shear stress and prevent bleeding.[48-50] MD simulations have been used to predict the range of forces that thrombi are exposed to within the blood.[26] The extensibility of fibrin involves unfolding of the coiled-coil regions and γ-chain C-terminal domain.[51,52] The lost tangent, a ratio of loss modulus over storage modulus (G″/G′), was increased for γDEK, indicating that these clots were more viscous and, therefore, more readily deformable overall. This is intriguing, because the altered clot structure for γDEK (denser network and smaller pores) would imply that the clot should be stiffer overall, which has been previously described for these types of clot networks.[53,54] However, the change of 2 residues involved in the catch-slip bonding character and 1 residue involved in protofibril packing in γDEK likely leads to increased deformation within the fibrin fibers of the variants and the production of weaker clots, resulting from decreased protofibril packaging and increased protofibril slippage despite the denser overall network structure.

Fibrinogen γD297N resides in a γ294-301-residue stretch called movable flap that is associated with low-affinity calcium binding,[55] more commonly known as the γ2 site. Previous modifications of the γ2 site via recombinant fibrinogens γD298A and γD301A caused minor functional abnormalities.[56] Here we show that γD297N has an effect on the functional properties of fibrinogen, which we attribute to attenuation of the catch regime of the A:a catch-slip bond. In addition, high affinity calcium binding sites that involve residues γD318, γD320, γG324, and γF322[57] are affected in fibrinogen Des Moines (γD320 deletion)[58] and Vlissingen (γD319 and γD320 deletion),[59] thus resulting in abnormal clots highlighting the importance of residues within this region. Not surprisingly, the results of MD simulations showed that γE323Q fibrinogen results in abolition of the catch-slip bonds. Further clinical evidence for the relevance of this region comes from several variants in residues interacting with γD297, γE323, or γK356. Fibrinogen Miami[60] (BβD61G) displays delayed onset and rate of polymerization and BβD61has been shown to form inter-protofibril contacts with γK356.[26] BβH67 interacts with γD297, and BβH67L (fibrinogen Sumperk) resulted in hypofibrinogenemia associated with bleeding, delayed polymerization, and abnormal clot properties.[61] Residue γE323 interacts with Bβ58, which is abnormal in fibrinogen Christchurch V (BβK58 > frameshift41aa-stop) resulting in a truncated β chain,[62] but in this case, the clinical phenotype is likely the result of the truncated protein.

The all-atomic MD simulations carried out in this study showed that γD297N and γE323Q result in a lower unbinding force (weaker slip bond character) compared with WT when knob A was pulled from hole a, indicating the abolition of the high-affinity catch bonds.[27] However, γK356Q formed catch-slip bonds at a similar rate as WT but persisted to display altered polymerization and clot structure. To investigate this unexpected result, we reconstructed the protofibril structure in silico. We found that γK356Q was relatively exposed to solvent, and any mutation in this region would likely disturb lateral packing interactions at the inter-protofibril level involving residues γ350-360 and γ370-380 as described.[19] In respect to variant γDEK, molecular modeling showed absence of the catch-slip bond character that is expected as they are also absent from γD297N and γE323Q. Across

Figure 6 (continued) (C) and top view (D) of a structural fragment of 2-stranded fibrin oligomer inside its hydrodynamic volume, displaying the α chain (in red color), β chain (in blue), and γ chain (in green). Also shown are the D:D self-association interface, the D:E:D complex with the A:a and B:b knob-hole bonds, the coiled coils, and carbohydrate moieties. These structures reveal the positions of mutated residues relative to the body of fibrin oligomer, which can be correlated with their propensities to form the intra-protofibril vs inter-protofibril contacts. (E) The same structure as in panel D but with another protofibril added to the picture to help visualize the lateral packing with the inter-protofibril contacts corresponding to the crystal contacts in structure 1FZC[19] from the protein data bank.

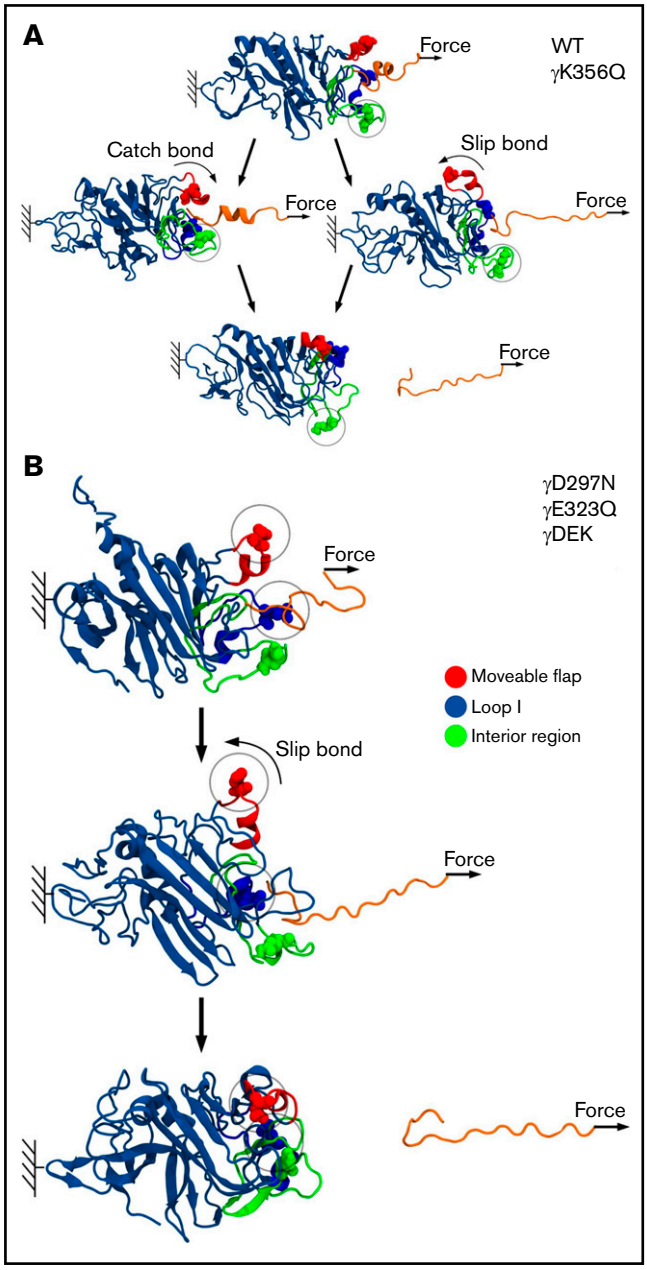

Figure 7. Molecular mechanism of A:a knob-hole bond rupture. Conformational transitions and remodeling of the A:a binding interface are exemplified for single-point mutants γK356Q (green balls) and γD297N (red balls), which result in kinetic partitioning into the bi-phasic catch-slip-type (A) and slip-type bond rupture pathways (B). The atomic structure of the A:a knob-hole complex (in ribbon representation) showing knob A (residues α17-36; in orange color) and hole a with the interior region (γ335-365; in green), loop I (γ315-330; in blue), and movable flap (γ295-305; in red). The pulling force is applied to residue α36 in knob A (small arrows), whereas residue γ159 in the γ-nodule is constrained (color denotation as in Figure 6).

most experiments, γDEK was structurally and functionally most different from WT, suggesting a cumulative effect from the disruption of A:a catch-slip bonds through γD297N and γE323Q and the disruption of lateral packing interactions via γK356Q. This leads to a greater impact on polymerization rate, fiber thickness, and clot density, resulting in clots that are more readily deformable. Hence, the results of structural analysis provide new evidence for the role of movable flap in formation of extended binding with knob A, in dynamic regulation of A:a interactions and transition from the catch bonds to slip bonds in fibrin.

Through state-of-the-art in vitro and in silico methods, our data indicate that A:a knob-hole bonds involved in fibrin polymerization are modified via catch-slip bond mechanisms involving residues γD297 and γE323. We found that small changes within the side chains of these key residues influence catch-slip bonds and lower the rupture force of dissociation of knob A from hole a, which subsequently amplifies into changes in overall clot structure and mechanical properties, with implications for clot stability and thus hemostasis and thrombosis. In pathophysiological circumstances, for example, thrombosis, this could be important as the catch-bond character allows the bonds to counterintuitively strengthen under shear stresses from the flowing blood, possibly preventing embolization. Although not involved in the A:a catch bond formation, residue γK356 was implicated in lateral packing, and when both catch-slip bonds and packing interactions are disturbed, the clot mechanics are affected with clots becoming more readily deformable. Together, these results indicate the involvement of extended interactions near non-covalent A:a catch-slip bonds in clot formation and stability. Future studies should explore how these results impact thrombosis and thromboembolism.

Acknowledgments

The authors thank Martin Fuller, University of Leeds, for assistance in critical point drying of SEM samples.

This study was supported by a British Heart Foundation Studentship for N.L.A. (FS/15/37/31513). N.L.A. was also supported by the British Society of Haemostasis and Thrombosis and the University of Leeds for a J-1 Research exchange collaboration visit to the laboratory of Valeri Barsegov (University of Massachusetts Lowell, MA). The R.A.S.A. laboratory is supported by British Heart Foundation Programme (RG/13/3/30104 and RG/18/11/34036 renewal) and project (PG/16/60/32292) grants. The V.B. laboratory is supported by National Institutes of Health grant R01HL148227 and National Science Foundation grant MCB-2027530.

Authorship

Contribution: N.L.A. performed most of the work, alongside C.D., A.Z., S.R.B., H.R.M., and M.M.D.; M.M.D., C.D., N.L.A., S.D.A.C., V.B., and R.A.S.A. designed the study; N.L.A., C.D., A.Z., V.B., and R.A.S.A. wrote the manuscript; and all authors reviewed the manuscript.

Conflict-of-interest disclosure: The authors declare no competing financial interests.

ORCID profiles: N.L.A., 0000-0002-7073-825X; C.D., 0000-0002-4870-6542; M.M.D., 0000-0003-1502-1421; S.D.A.C., 0000-0003-2500-5724; V.B., 0000-0003-1994-3917; R.A.S.A., 0000-0002-6310-5745.

Correspondence: Robert Ariëns, Discovery and Translational Science Department, Leeds Institute of Cardiovascular and Metabolic Medicine, University of Leeds, LS2 9JT, UK; e-mail: r.a.s.ariens@leeds.ac.uk.

References

1. Spronk HMH, van der Voort D, Ten Cate H. Blood coagulation and the risk of atherothrombosis: a complex relationship. *Thromb J.* 2004;2(1):12.
2. Phillippe HM. Overview of venous thromboembolism. *Am J Manag Care.* 2017;23(20 Suppl):S376-S382.
3. Staton CA, Brown NJ, Lewis CE. The role of fibrinogen and related fragments in tumour angiogenesis and metastasis. *Expert Opin Biol Ther.* 2003;3(7):1105-1120.
4. Macrae FL, Duval C, Papareddy P, et al. A fibrin biofilm covers blood clots and protects from microbial invasion. *J Clin Invest.* 2018;128(8): 3356-3368.
5. Prasad JM, Gorkun OV, Raghu H, et al. Mice expressing a mutant form of fibrinogen that cannot support fibrin formation exhibit compromised antimicrobial host defense. *Blood.* 2015;126(17):2047-2058.
6. Zhmurov A, Protopopova AD, Litvinov RI, et al. Structural basis of interfacial flexibility in fibrin oligomers. *Structure (London, England: 1993).* 2016; 24(11):1907-1917.
7. Hall CE, Slayter HS. The fibrinogen molecule: its size, shape, and mode of polymerization. *J Biophys Biochem Cytol.* 1959;5(1):11-16.
8. Veklich YI, Gorkun OV, Medved LV, Nieuwenhuizen W, Weisel JW. Carboxyl-terminal portions of the alpha chains of fibrinogen and fibrin. Localization by electron microscopy and the effects of isolated alpha C fragments on polymerization. *J Biol Chem.* 1993;268(18):13577-13585.
9. Lorand L, Middlebrook WR. The action of thrombin on fibrinogen. *Biochem J.* 1952;52(2):196-199.
10. Spraggon G, Everse SJ, Doolittle RF. Crystal structures of fragment D from human fibrinogen and its crosslinked counterpart from fibrin. *Nature.* 1997;389(6650):455-462.
11. Kostelansky MS, Betts L, Gorkun OV, Lord ST. 2.8 A crystal structures of recombinant fibrinogen fragment D with and without two peptide ligands: GHRP binding to the "b" site disrupts its nearby calcium-binding site. *Biochemistry.* 2002;41(40):12124-12132.
12. Everse SJ, Spraggon G, Veerapandian L, Riley M, Doolittle RF. Crystal structure of fragment double-D from human fibrin with two different bound ligands. *Biochemistry.* 1998;37(24):8637-8642.
13. Erickson HP, Fowler WE. Electron microscopy of fibrinogen, its plasmic fragments and small polymers. *Ann N Y Acad Sci.* 1983;408(1 Molecular Bio):146-163.
14. Chernysh IN, Nagaswami C, Weisel JW. Visualization and identification of the structures formed during early stages of fibrin polymerization. *Blood.* 2011;117(17):4609-4614.
15. Litvinov RI, Gorkun OV, Galanakis DK, et al. Polymerization of fibrin: direct observation and quantification of individual B:b knob-hole interactions. *Blood.* 2007;109(1):130-138.
16. Litvinov RI, Yakovlev S, Tsurupa G, Gorkun OV, Medved L, Weisel JW. Direct evidence for specific interactions of the fibrinogen alphaC-domains with the central E region and with each other. *Biochemistry.* 2007;46(31):9133-9142.
17. Protopopova AD, Barinov NA, Zavyalova EG, Kopylov AM, Sergienko VI, Klinov DV. Visualization of fibrinogen αC regions and their arrangement during fibrin network formation by high-resolution AFM. *J Thromb Haemost.* 2015;13(4):570-579.
18. Protopopova AD, Litvinov RI, Galanakis DK, et al. Morphometric characterization of fibrinogen's αC regions and their role in fibrin self-assembly and molecular organization. *Nanoscale.* 2017;9(36):13707-13716.
19. Yang Z, Mochalkin I, Doolittle RF. A model of fibrin formation based on crystal structures of fibrinogen and fibrin fragments complexed with synthetic peptides. *Proc Natl Acad Sci USA.* 2000;97(26):14156-14161.
20. Weisel JW, Medved L. The structure and function of the alpha C domains of fibrinogen. *Ann N Y Acad Sci.* 2001;936(1):312-327.
21. Collet JP, Moen JL, Veklich YI, et al. The alphaC domains of fibrinogen affect the structure of the fibrin clot, its physical properties, and its susceptibility to fibrinolysis. *Blood.* 2005;106(12):3824-3830.
22. Jansen KA, Zhmurov A, Vos BE, et al. Molecular packing structure of fibrin fibers resolved by X-ray scattering and molecular modeling. *Soft Matter.* 2020;16(35):8272-8283.
23. Blombäck B, Hessel B, Hogg D, Therkildsen L. A two-step fibrinogen-fibrin transition in blood coagulation. *Nature.* 1978;275(5680):501-505.
24. Bowley SR, Lord ST. Fibrinogen variant BbetaD432A has normal polymerization but does not bind knob "B". *Blood.* 2009;113(18):4425-4430.
25. Geer CB, Tripathy A, Schoenfisch MH, Lord ST, Gorkun OV. Role of 'B-b' knob-hole interactions in fibrin binding to adsorbed fibrinogen. *J Thromb Haemost.* 2007;5(12):2344-2351.
26. Kononova O, Litvinov RI, Zhmurov A, et al. Molecular mechanisms, thermodynamics, and dissociation kinetics of knob-hole interactions in fibrin. *J Biol Chem.* 2013;288(31):22681-22692.
27. Litvinov RI, Kononova O, Zhmurov A, et al. Regulatory element in fibrin triggers tension-activated transition from catch to slip bonds. *Proc Natl Acad Sci USA.* 2018;115(34):8575-8580.
28. Feller T, Connell SDA, Ariens RA. Why fibrin biomechanical properties matter for hemostasis and thrombosis. *J Thromb Haemost.* 2021.
29. Tutwiler V, Maksudov F, Litvinov RI, Weisel JW, Barsegov V. Strength and deformability of fibrin clots: Biomechanics, thermodynamics, and mechanisms of rupture. *Acta Biomater.* 2021;131:355-369.

30. Duval C, Allan P, Connell SD, Ridger VC, Philippou H, Ariëns RA. Roles of fibrin α- and γ-chain specific cross-linking by FXIIIa in fibrin structure and function. *Thromb Haemost.* 2014;111(5):842-850.

31. Duval C, Ali M, Chaudhry WW, Ridger VC, Ariëns RA, Philippou H. Factor XIII A-subunit V34L variant affects thrombus cross-linking in a murine model of thrombosis. *Arterioscler Thromb Vasc Biol.* 2016;36(2):308-316.

32. Domingues MM, Macrae FL, Duval C, et al. Thrombin and fibrinogen γ′ impact clot structure by marked effects on intrafibrillar structure and protofibril packing. *Blood.* 2016;127(4):487-495.

33. Carr ME Jr, Hermans J. Size and density of fibrin fibers from turbidity. *Macromolecules.* 1978;11(1):46-50.

34. Yeromonahos C, Polack B, Caton F. Nanostructure of the fibrin clot. *Biophys J.* 2010;99(7):2018-2027.

35. Allan P, Uitte de Willige S, Abou-Saleh RH, Connell SD, Ariëns RA. Evidence that fibrinogen γ′ directly interferes with protofibril growth: implications for fibrin structure and clot stiffness. *J Thromb Haemost.* 2012;10(6):1072-1080.

36. Zhmurov A, Protopopova AD, Litvinov RI, Zhukov P, Weisel JW, Barsegov V. Atomic structural models of fibrin oligomers. *Structure.* 2018;26(6): 857-868.e4.

37. Zhmurov A, Dima RI, Kholodov Y, Barsegov V. Sop-GPU: accelerating biomolecular simulations in the centisecond timescale using graphics processors. *Proteins.* 2010;78(14):2984-2999.

38. Zhmurov A, Rybnikov K, Kholodov Y, Barsegov V. Generation of random numbers on graphics processors: forced indentation in silico of the bacteriophage HK97. *J Phys Chem B.* 2011;115(18):5278-5288.

39. Ferrara P, Apostolakis J, Caflisch A. Evaluation of a fast implicit solvent model for molecular dynamics simulations. *Proteins.* 2002;46(1):24-33.

40. Weisel JW, Dempfle CH. Fibrinogen structure and function. In: Marder VJ, Aird WC, Bennett JS, Schulman S, White GC II, eds. *Hemostasis and Thrombosis Basic Principles and Clinical Practice.* Philadelphia: Lippincott Williams & Wilkins; 2012:254-271.

41. Mutch NJ, Engel R, Uitte de Willige S, Philippou H, Ariëns RAS. Polyphosphate modifies the fibrin network and down-regulates fibrinolysis by attenuating binding of tPA and plasminogen to fibrin. *Blood.* 2010;115(19):3980-3988.

42. Hethershaw EL, Cilia La Corte AL, Duval C, et al. The effect of blood coagulation factor XIII on fibrin clot structure and fibrinolysis. *J Thromb Haemost.* 2014;12(2):197-205.

43. Undas A, Ariëns RA. Fibrin clot structure and function: a role in the pathophysiology of arterial and venous thromboembolic diseases. *Arterioscler Thromb Vasc Biol.* 2011;31(12):e88-e99.

44. Wolberg AS. Thrombin generation and fibrin clot structure. *Blood Rev.* 2007;21(3):131-142.

45. Weisel JW, Nagaswami C. Computer modeling of fibrin polymerization kinetics correlated with electron microscope and turbidity observations: clot structure and assembly are kinetically controlled. *Biophys J.* 1992;63(1):111-128.

46. Lim BB, Lee EH, Sotomayor M, Schulten K. Molecular basis of fibrin clot elasticity. *Structure.* 2008;16(3):449-459.

47. Maksudov F, Daraei A, Sesha A, Marx KA, Guthold M, Barsegov V. Strength, deformability and toughness of uncrosslinked fibrin fibers from theoretical reconstruction of stress-strain curves. *Acta Biomater.* 2021;136:327-342.

48. Ferry JD, Miller M, Shulman S. The conversion of fibrinogen to fibrin. VII. Rigidity and stress relaxation of fibrin clots, eff. of calcium. *Arch Biochem Biophys.* 1951;34(2):424-436.

49. Collet J-P, Shuman H, Ledger RE, Lee S, Weisel JW. The elasticity of an individual fibrin fiber in a clot. *Proc Natl Acad Sci USA.* 2005;102(26): 9133-9137.

50. Ma TM, VanEpps JS, Solomon MJ. Structure, mechanics, and instability of fibrin clot infected with staphylococcus epidermidis. *Biophys J.* 2017; 113(9):2100-2109.

51. Guthold M, Liu W, Sparks EA, et al. A comparison of the mechanical and structural properties of fibrin fibers with other protein fibers. *Cell Biochem Biophys.* 2007;49(3):165-181.

52. Zhmurov A, Brown AE, Litvinov RI, Dima RI, Weisel JW, Barsegov V. Mechanism of fibrin(ogen) forced unfolding. *Structure.* 2011;19(11): 1615-1624.

53. Collet JP, Allali Y, Lesty C, et al. Altered fibrin architecture is associated with hypofibrinolysis and premature coronary atherothrombosis. *Arterioscler Thromb Vasc Biol.* 2006;26(11):2567-2573.

54. Konings J, Govers-Riemslag JW, Philippou H, et al. Factor XIIa regulates the structure of the fibrin clot independently of thrombin generation through direct interaction with fibrin. *Blood.* 2011;118(14):3942-3951.

55. Everse SJ, Spraggon G, Veerapandian L, Doolittle RF. Conformational changes in fragments D and double-D from human fibrin(ogen) upon binding the peptide ligand Gly-His-Arg-Pro-amide. *Biochemistry.* 1999;38(10):2941-2946.

56. Kostelansky MS, Lounes KC, Ping LF, Dickerson SK, Gorkun OV, Lord ST. Probing the gamma2 calcium-binding site: studies with gammaD298,301A fibrinogen reveal changes in the gamma294-301 loop that alter the integrity of the "a" polymerization site. *Biochemistry.* 2007;46(17):5114-5123.

57. Yee VC, Pratt KP, Côté HCF, et al. Crystal structure of a 30 kDa C-terminal fragment from the γ chain of human fibrinogen. *Structure.* 1997;5(1): 125-138.

58. Brennan SO, Davis RL, Mosesson MW, Hernandez I, Lowen R, Alexander SJ. Congenital hypodysfibrinogenaemia (Fibrinogen Des Moines) due to a gamma320Asp deletion at the Ca2+ binding site. *Thromb Haemost.* 2007;98(2):467-469.

59. Koopman J, Haverkate F, Briët E, Lord ST. A congenitally abnormal fibrinogen (Vlissingen) with a 6-base deletion in the gamma-chain gene, causing defective calcium binding and impaired fibrin polymerization. *J Biol Chem.* 1991;266(20):13456-13461.

60. Galanakis DK, Spitzer S, Ledford M, Henschen A. Fibrinogen Miami: a Bb61 Asp rGly substitution associated with impaired fibrin polymerization. *Fibrinolysis.* 1996;10:7.

61. Kotlín R, Sobotková A, Riedel T, et al. Acquired dysfibrinogenemia secondary to multiple myeloma. *Acta Haematol.* 2008;120(2):75-81.

62. Brennan SO, Mosesson MW, Lowen R, Siebenlist KR, Matsunaga A. Hypofibrinogenaemia resulting from novel single nucleotide deletion at codon Bbeta58 (3404del A) associated with thrombotic stroke in infancy. *Thromb Haemost.* 2006;95(4):738-739.